Preparation of ternary alloy libraries for high-throughput screening of material properties by means of thick film deposition and interdiffusion: Benefits and limitations

A. Rar[a)]
Oak Ridge National Laboratory, Metals and Ceramics Division, Oak Ridge, Tennessee 37831 and Department of Materials Science and Engineering, University of Tennessee, Knoxville, Tennessee

E. D. Specht
Oak Ridge National Laboratory, Metals and Ceramics Division, Oak Ridge, Tennessee 37831

E. P. George
Oak Ridge National Laboratory, Metals and Ceramics Division, Oak Ridge, Tennessee 37831 and Department of Materials Science and Engineering, Knoxville, Tennessee

M. L. Santella
Oak Ridge National Laboratory, Metals and Ceramics Division, Oak Ridge, Tennessee 37831

G. M. Pharr
Oak Ridge National Laboratory, Metals and Ceramics Division, Oak Ridge, Tennessee 37831 and Department of Materials Science and Engineering, Knoxville, Tennessee

(Received 8 October 2003; accepted 19 January 2004; published 23 July 2004)

Several techniques have been investigated for making alloy libraries for combinatorial materials development. In this investigation, we demonstrate a method for Ni–Fe–Cr ternary alloy library preparation by deposition of three layers of different metals with a linear thickness gradient rotated by 120° for each layer. The layers were interdiffused and alloyed by annealing in vacuum. The resulting specimens were analyzed and compared with the well-known phase diagram for this system by means of rapid x-ray diffraction mapping with synchrotron radiation. © *2004 American Vacuum Society.* [DOI: 10.1116/1.1692366]

I. INTRODUCTION

The development of the methods for high throughput analysis of binary, ternary, and quarternary alloys is a subject of great interest in materials science.[1–5] The main issues limiting wide application of combinatorial methods to alloy design are: (i) effective preparation of alloy libraries; (ii) how well the libraries reproduce the relevant properties of the bulk materials; and (iii) how the properties of these libraries can be rapidly assessed. Here, we investigate one way to achieve this using Ni–Fe–Cr as a model ternary alloy system. This system was selected because it is the basis of a wide variety of commercially important alloys such as stainless steel. As such, it has been extensively studied, and the structure and properties are well known.

The main focus of this article is alloy library preparation. Several techniques have been used to make ternary alloy libraries for combinatorial materials development including: (i) codeposition of materials from 2 or 3 different sources, (the "concentration spread method");[3,6–8] (ii) preparation of multilayer thin films with thickness gradients in different directions that are subsequently alloyed by solid state diffusion;[9,10] and (iii) the diffusion multiple approach wherein an assembly of different metal blocks is solid-state annealed at high temperatures to allow for thermal interdiffusion.[11,12] Each method has its own limitations. In the first, the element distribution is nonlinear, the film thickness is not constant, and regions with low concentrations of one or more elements are difficult to achieve. In the second, synthesis of thick films may be a problem because of the time needed to deposit large numbers of layers. The third method is constrained by the relatively small diffusion lengths over which interdiffusion takes place, which leads to significant composition variations over small length scales.

In this article, we present a different method for alloy library preparation based on deposition and interdiffusion of relatively thick layers. The benefits and limitations are outlined and discussed.

II. EXPERIMENT

Specimens of Ni–Fe–Cr were prepared by depositing films onto 5 cm diameter circular sapphire substrates followed by annealing in vacuum to interdiffuse the layers. Substrates with three different orientations were used: (0001), $(11\bar{2}0)$, and $(1\bar{1}02)$. The latter two orientations were found to suppress texture formation and therefore simplify structural analysis by x-ray diffraction (XRD).

Deposition was performed in an electron beam evaporation system equipped with a sliding shutter and a sample rotation stage. A typical background pressure was about 10^{-6} Torr, and the deposition rate measured with a quartz microbalance was about 3 nm/s for Cr and about 0.3 nm/s for Fe and Ni. Layers of Cr, Fe, and Ni were sequentially deposited using the sliding shutter to create a thickness gradient in each layer. The shutter was moved at a constant rate such that the thicknesses increased linearly with position to a

[a)]Author to whom correspondence should be addressed; electronic mail: rara@ornl.gov

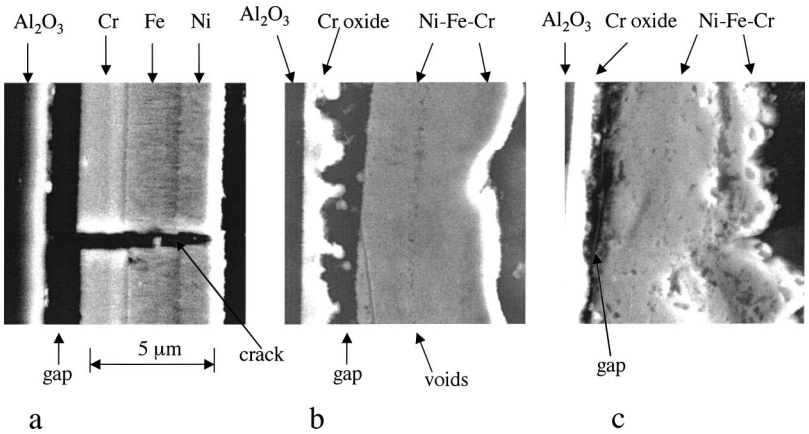

FIG. 1. Cross-sectional SEM images of Cr/Fe/Ni sample: as deposited (a) and after annealing in vacuum at 825 °C for 2 h 10 min (b), and 19 h 30 min (c).

maximum of about 1.7 μm on the thick end. After finishing a layer, the sample was rotated by 120° about the substrate center, and a layer of a different alloying component was deposited. The total thickness of the deposited layers was limited by the maximum thickness measurable by the quartz microbalance (about 5 μm).

After deposition, the layers were interdiffused by annealing in a vacuum using annealing times and temperatures which will be discussed later. After annealing, the sample was slowly cooled to room temperature in about 12 h, with the initial cooling to 500 °C taking about 1 h. The resulting sample had a triangular region with a constant thickness of about 1.7 μm and compositions spanning the entire ternary phase diagram. In the sample preparation we rely on the total film thickness determined during the deposition and had no options to confirm it in independent measurements. Cr/Fe/Ni samples with uniform individual layer thicknesses of about 1.7 μm each were also prepared to examine the extent of the interdiffusion during annealing.

The quality of the alloyed specimens was examined using cross sectional scanning electron microscopy (SEM), angular resolved x-ray fluorescence, scanning Auger electron spectroscopy (AES), and x-ray diffraction (XRD) including diffraction mapping using synchrotron radiation. Samples for cross-sectional SEM were cut from the wafer, mounted in epoxy, polished, and carbon coated. Angular resolved x-ray fluorescence measurements were made with a Cu rotating anode operating at 50 kV and 100 mA. Cu $K\beta$ radiation was employed using a sagitally focusing bent graphite monochromator. The angle of incidence θ on the sample was varied from 2.5° to 35°, exciting fluorescence from the Cr, Fe, and Ni atoms in the sample. The fluorescence was analyzed using a Li-drifted Si detector in a symmetrical θ-2θ geometry, that is, the fluorescence detector was positioned to detect at a reflected angle equal to the angle of the incident x-ray beam. For a layer of uniform composition, this results in no variation of fluorescent intensity with changes in 2θ (in the limit of a thick layer), while for a compositionally stratified layer, fluorescence from the near-surface region is stronger at smaller 2θ. This provides a useful way to explore the through-thickness homogeneity of the specimens after annealing.

Details of the structural and chemical mapping using synchrotron radiation can be found elsewhere.[13] Briefly, experiments were conducted at the 33 BM beam line of the Advance Photon Source using 12 keV x rays focused to give a 1 mm^2 footprint on the sample. The sample was rastered in the x-y plane of the sample with 1 mm steps to provide composition and structural information at each sample point. Structure was determined using diffracted x rays collected with a 1024×1024 pixel CCD camera. Chemical composition was measured by x-ray fluorescence using a silicon detector. The area under each peak of the fluorescence spectrum was found by least-squares fitting to Gaussian line shapes. While the measurement is precise to within a 1% absolute variation in composition, the relative systematic error was estimated to be about 10%. The incident angle for diffraction and takeoff angle for fluorescence were about 75° from the sample normal.

III. RESULTS AND DISCUSSION

The most important requirement for the ternary alloy library specimens is complete through-thickness mixing of the metal layers. To achieve this, the temperature range selected for annealing was 825–875 °C. At higher temperatures, Cr evaporation was significant, and for lower temperatures, delamination of the film from the substrate became a problem, as will be discussed below.

The time required for the layers to fully interdiffuse was first roughly estimated based on published diffusion data.[14,15] For the temperature range 825–875 °C, typical diffusion coefficients for the Ni–Fe–Cr system are of the order of 10^{-16} $m^2 s^{-1}$, which suggests that times of about 10 h are required for 1.7 μm films. Studies to establish the annealing conditions more precisely were conducted using specimens in which the Cr, Fe, and Ni layers were uniform. Each layer had a thickness of 1.7 μm, with the layer closest to the substrate being Cr followed by Fe and Ni. At this composition, a homogeneous single fcc phase is expected at equilibrium.

Figure 1 shows typical cross section SEM images of the "as-deposited" sample [Fig. 1(a)] and the sample after annealing in vacuum at 825 °C for 2 h 10 min [Fig. 1(b)] and 19 h 30 min [Fig. 1(c)]. In Fig. 1(a), all three as-deposited

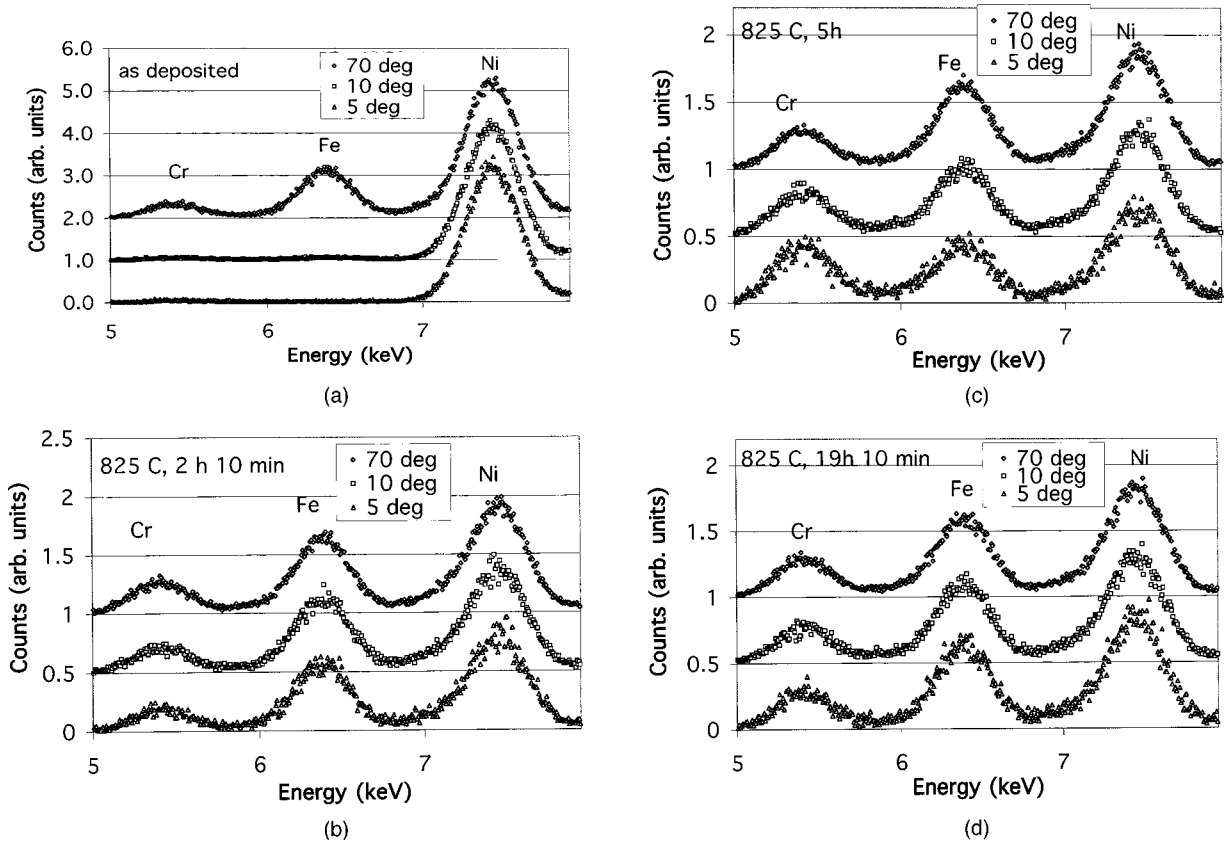

FIG. 2. Angular resolved x-ray fluorescence spectra for: (a) an as-deposited Cr/Fe/Ni sample, and after annealing at 825 °C for (b) 2 h 10 min; (c) 5 h, and (d) 19 h 10 min.

metal layers are distinguishable in the SEM image, and the interfaces between the layers are relatively flat. A gap between the substrate and film formed as a result of film delamination due to epoxy shrinkage during mounting. A crack in the film may be formed in the result of the internal film stress. After 2 h 10 min of annealing [Fig. 1(b)], the appearance of the layers changes dramatically. Two different areas separated by a gap are observed. Based on EDS measurements of the chemical constituents, the outerlayer is a relatively uniform mixture of Ni–Fe–Cr, while the thin rough innerlayer on the substrate consists mainly of chromium oxide. The oxide, which presumably originates from oxygen dissolved in the film, oxygen introduced during annealing, and/or oxygen in the substrate, ties up some of the chromium and therefore reduces the local chromium concentration in the outer alloyed layer. The chromium oxide is well-adhered to the substrate. The gap between alloy and Cr oxide formed again mainly as result of epoxy shrinkage. Note, however, that although the innersurface of the alloy layer is relatively flat, the Cr oxide surface is extremely rough, suggesting some void formation during interdiffusion. Figure 1(c) shows that the roughness of and porosity of the outer Ni–Fe–Cr layer increase with annealing time. Thus, in order to obtain alloy libraries of high structural quality, very long annealing times may not be desirable.

The through-thickness chemical uniformity of the interdiffused layers was analyzed using angular resolved x-ray fluorescence. Typical results are shown in Fig. 2, which presents fluorescence spectra for an as-deposited specimen [Fig. 2(a)] and three specimens annealed in vacuum at 825 °C for periods of 2 h 10 min [Fig. 2(b), 5 h [Fig. 2(c)], and 19 h 10 min [Fig. 2(d)]. Each plot includes spectra obtained at $2\theta = 5°$, 10°, and 70°. For the specimens in Figs. 2(b) and 2(d), the pressure in the furnace prior to annealing was 7×10^{-7} Torr. For the specimen in Fig. 2(c), the pressure was slightly higher at 6×10^{-6} Torr.

The data in Fig. 2(a) illustrate the utility of the angular resolved fluorescence technique. For $2\theta = 5°$ and 10°, no Cr or Fe $K\alpha$ peaks are observed because the Cr and Fe are buried beneath the Ni. A simple analysis shows that the depth of fluorescence signal is only about 0.07 μm for $2\theta = 5°$ and 0.14 μm for $2\theta = 10°$. Thus, only the Ni $K\alpha$ peak is observed, since the top Ni layer extends to a depth of about 1.7 μm. For $2\theta = 70°$, the penetration depth increases enough that both Cr and Fe peaks begin to emerge. In contrast, Fig. 2(b) shows that after 2 h 10 min, peaks from all three elements appear at each 2θ. How homogeneous the mixture is then depends on the how the relative peak heights vary with 2θ. In Fig. 2(b), the ratio of the Fe to Ni peak heights does not change from $2\theta = 5°$ to 70°, but the ratio of Cr to Ni signal increases by 20% when 2θ changes from 5° to 10°. Thus, the sample surface is deficient in Cr and full homogenization has not been achieved. No changes in the relative signal heights are observed after 19 h 10 min of annealing

[Fig. 2(d)], indicating complete interdiffusion of the metals. The sample annealed 5 h [Fig. 2(c)] in the worse vacuum conditions produced a higher Cr peak at $2\theta = 5°$ than at 10° or 70°, suggesting preferential Cr segregation at the surface. This may be due to the formation of Cr oxide on the surface as the result of the poorer vacuum conditions.

Similar SEM and x-ray fluorescence analyses were performed on samples prepared at different temperatures and annealing times. It was found that annealing below 800 °C frequently led to film delamination and annealing above 900 °C gave rise to unacceptable evaporation of Cr. In general, the best specimens were produced in the temperature range 850–875 °C at an annealing time of about 5 h. In an attempt to reduce oxidation during annealing, we also performed interdiffusion using encapsulation of the sample in quartz tubes backfilled with high purity Ar or forming gas and by pressing two specimen surfaces together. However, neither technique produced significant improvements. Both for the encapsulated and unencapsulated specimens AES ion sputtering depth profiling showed that the sample surface after annealing in high vacuum had an oxide surface layer with thickness of no more than a few nanometers. We may speculate, therefore, that significant oxygen contamination does not occur during the annealing step.

The structural and chemical quality of the ternary alloy libraries was examined with scanning XRD. Results after annealing for 5 h and 3 h 20 min at 875 °C, and after 2 h 10 min at 825 °C are shown in Figs. 3(a)–3(c), respectively. Theoretically calculated ternary alloy phase diagrams at 875 and 700 °C are shown in Figs. 4(a) and 4(b), respectively. The calculations were performed using the PANDAT™ Software Package[16] and SSOL2–SGTE Solutions Database.[17,18] The phase diagrams measured from the experimental libraries are in reasonably good agreement with the theoretical behavior with all the relevant phases appearing and their locations on the diagram being approximately correct. There are, however, a few notable differences. At compositions near the Ni–Cr binary side of the diagram, all the measured libraries give the correct location of γ (fcc) and $\alpha+\gamma$ (bcc + fcc) phases, but the extent of the α (bcc) phase is displaced to higher Ni concentrations than what is predicted by the calculated diagram [see Fig. 4(a)]. For compositions near the Fe–Ni binaries the extent of α (bcc) phase is also greater than expected.

The most complex region in the ternary diagram [see Fig. 4(a)] is located between the Fe and Cr corners at Cr concentrations from 20 to 70 at. % and Fe concentrations from 25 to 65 at. % due to the appearance of the tetragonal intermetallic σ phase. In this region, four different phase fields are expected based on the calculated 875 °C diagram: σ (tetragonal intermetallic) and combination of σ with α, γ, and the $\alpha + \gamma$ phases. The position and size of these phase fields are not reproduced well from library to library [Figs. 3(a) and 3(b)] and deviate from the theoretical diagram. The insufficient annealing time used for the library in Fig. 3(c) leads to the complete absence of single phase σ region in the diagram. However other regions in the phase diagram were reproduced well for this annealing condition. We may speculate, therefore, that σ phase formation is relatively slow compared to the other phase.

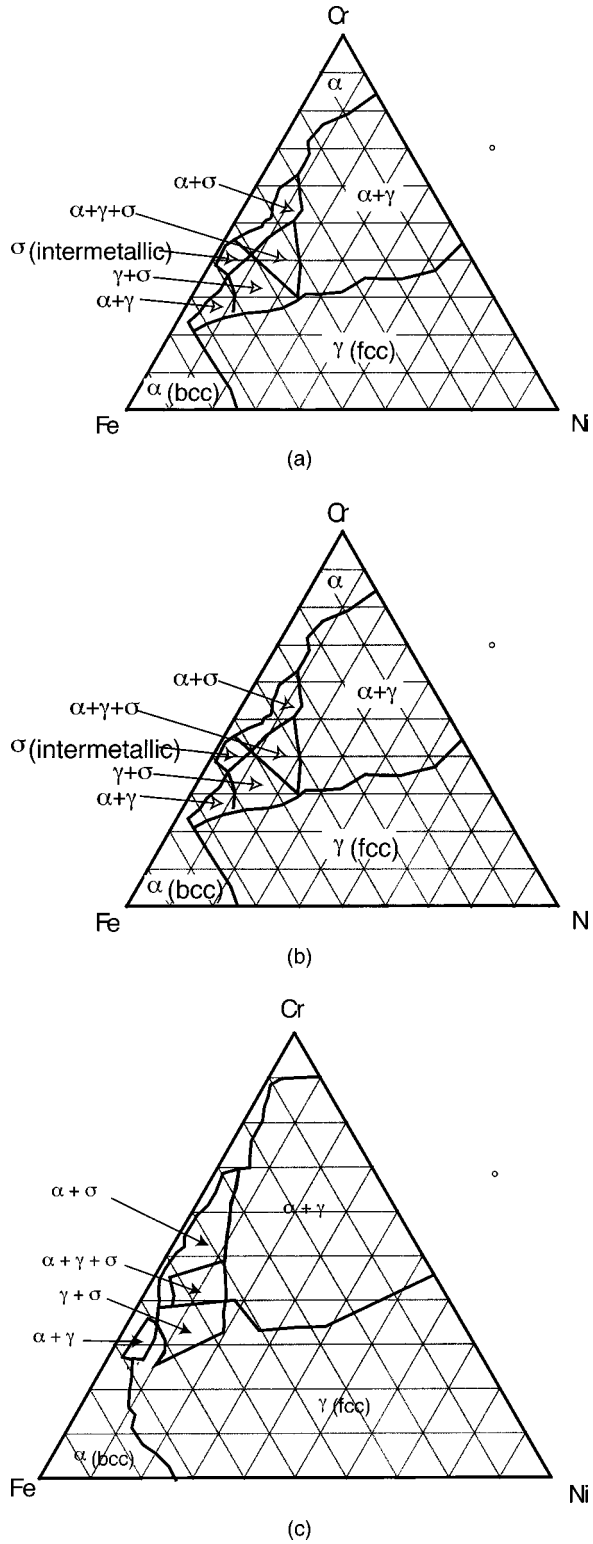

FIG. 3. Ternary phase diagrams measured after annealing at 875 °C for (a) 5 h, (b) 3 h 20 min, and at 825 °C at 2 h 10 min (c).

Many sources of error may contribute to the shifts in the observed phase locations. One is the lateral extent of the

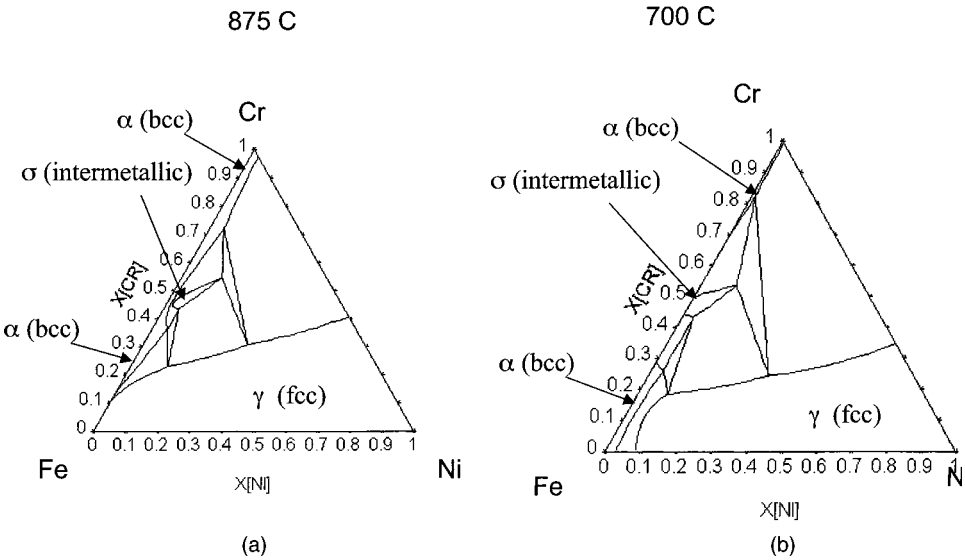

FIG. 4. Theoretically predicted ternary phase diagrams at (a) 875 °C, and (b) 700 °C.

phase on the diagram and whether it is large enough to be experimentally measured by the XRD techniques. For example, the width of the σ phase in the library must be about 1–2 mm [Fig. 4(a)], so that it is comparable to the lateral resolution of the XRD measurements. This resolution could be improved at the cost of longer experimental time. Another problem results from changes in equilibrium during sample cooling. In this regard, it is instructive to compare the calculated ternary diagram at 875 °C [Fig. 4(a)] to that at 700 °C [Fig. 4(b)]. Inspection shows that the phase field boundaries in problematic locations are indeed different. For example, the phase changes from (fcc) to (bcc) may occur during the cooling period in the Fe rich corner. Thus, the slow rate of cooling used during the experiments probably limits our ability to recreate true equilibrium conditions. This problem may be rectified by increasing the cooling rate. Impurities and influences of the substrate on film orientation and epitaxy are other possible sources of difficulty.

IV. CONCLUSIONS

Ni–Fe–Cr alloy libraries were prepared by depositing layers of Cr, Fe, and Ni on Al_2OO_3 substrates followed by 2–5 h of interdiffusion at 825–875 °C in high vacuum. The samples were examined with x-ray fluorescence, SEM, AES, and XRD. The chromium oxide formed at the interface between the deposited metals and the substrate, but the outer-layer (about 1 μm) of the metal film can be used as a ternary alloy library for property characterization. The library covered all possible compositions and compared generally well with the known ternary phase diagram.

ACKNOWLEDGMENTS

Research sponsored by the U.S. Department of Energy, Office of Energy Efficiency and Renewable Energy, Industrial Technologies Program, Industrial Materials for the Future, and by the Division of Materials Sciences and Engineering, Office of Basic Energy Sciences, under Contract No. DE-AC05-00OR22725 with UT-Battelle, LLC. The UNICAT facility at the Advanced Photon Source (APS) is supported by the University of Illinois at Urbana-Champaign, Materials Research Laboratory (U.S. DOE, the State of Illinois-IBHE-HECA, and the NSF), the Oak Ridge National Laboratory (U.S. DOE under contract with UT-Battelle LLC), the National Institute of Standards and Technology (U.S. Department of Commerce), and UOP LLC. The APS is supported by the U.S. DOE, Basic Energy Sciences, Office of Science under Contract No. W-31-109-ENG-38.

[1]K. Kennedy, T. Stefansky, G. Davy, V. F. Zackay, and E. R. Parker, J. Appl. Phys. **36**, 3808 (1965).
[2]J. J. Hanak, J. Mater. Sci. **5**, 9601 (1970).
[3]H. M. Christen, S. D. Silliman, and K. S. Harshavardhan, Rev. Sci. Instrum. **72**, 2673 (2001).
[4]P. C. Collins, R. Banerjee, S. Banerjee, and H. L. Fraser, Mater. Sci. Eng., A **352**, 118 (2003).
[5]E. B. Svedberg, R. J. M. van de Veerdonk, K. J. Howard, and L. D. Madsen, J. Appl. Phys. **93**, 5519 (2003).
[6]R. Cremer, S. Dondorf, M. Hauck, D. Horbach, M. Kaiser, S. Kyrsta, O. Kyrylov, E. Munstermann, M. Philipps, K. Reichert, and G. Strauch, Z. Metallkd. **92**, 1120 (2001).
[7]S. Kyrsta, R. Cremer, D. Neuschutz, M. Laurenzis, P. H. Bolivar, and H. Kurz, Thin Solid Films **398**, 379 (2001).
[8]H. M. Christen, S. D. Silliman, and K. S. Harshavardhan, Appl. Surf. Sci. **189**, 216 (2002).
[9]H. Chang, I. Takeuchi, and X. D. Xiang, Appl. Phys. Lett. **74**, 1165 (1999).
[10]Y. K. Yoo, T. Ohnishi, G. Wang, F. Duewer, X. D. Xiang, Y. S. Chu, D. C. Mancini, Y. Q. Li, and R. C. O'Handley, Intermetallics **9**, 541 (2001).
[11]J. C. Zhao, M. R. Jackson, L. A. Peluso, and L. N. Brewer, J. Miner. Metals Mater. Soc. **54**, 42 (2002).
[12]L. C. Zhao, M. R. Jackson, L. A. Peluso, and L. N. Brewer, MRS Bull. **27**, 324 (2002).
[13]E. D. Specht, A. Rar, G. M. Pharr, E. P. George, P. Zschack, H. Hong, and J. Ilavsky, J. Mater. Res. **18**, 2522 (2003).
[14]B. Josson, ISIJ Int. **35**, 1415 (1995).
[15]C. E. Campbell, W. J. Boettinger, and U. R. Kattner, Acta Mater. **50**, 775 (2002).
[16]S.-L. Chen, S. Daniel, F. Zhang, Y. A. Chang, X.-Y. Yan, F.-Y. Xie, R. Schmid-Fetzer, and W. A. Oates, CALPHAD: Comput. Coupling Phase Diagrams Thermochem. **26**, 175 (2002).
[17]"SSOL2–SGTE Solutions Database, v 2.0 (provided by ThermoCalc Software)," SGTE, 2002.
[18]*The SGTE Casebook: Thermodynamics at Work*, edited by K. Hack (The Institute of Materials, London, 1996), p. 227.